ACS SENSORS

pubs.acs.org/acssensors
Article

Multiplex Determination of Glycan Profiles on Urinary Prostate-Specific Antigen by Quartz-Crystal Microbalance Combined with Surface-Enhanced Raman Scattering

Laura Armero, Javier Plou, Pablo S. Valera, Sonia Serna, Isabel García,* and Luis M. Liz-Marzán*

Cite This: ACS Sens. 2024, 9, 4811−4821

ABSTRACT: Prostate cancer remains a major health concern, with prostate-specific antigen (PSA) being a key biomarker for its detection and monitoring. However, PSA levels often fall into a "gray zone", where PSA levels are not clearly indicative of cancer, thus complicating early diagnosis and treatment decisions. Glycosylation profiles, which often differ between healthy and diseased cells, have emerged as potential biomarkers to enhance the specificity and sensitivity of cancer diagnosis in these ambiguous cases. We propose the integration of two complementary techniques, namely quartz-crystal microbalance with dissipation (QCM-D) and surface-enhanced Raman scattering (SERS) to study PSA glycan profiles. QCM-D offers real-time operation, PSA mass quantification, and label-free detection with high sensitivity, as well as enhanced specificity and reduced cross-reactivity when using nucleic acid aptamers as capture ligands. Complementary SERS sensing enables the determination of the glycosylation pattern on PSA, at low concentrations and without the drawbacks of photobleaching, thereby facilitating multiplexed glycosylation pattern analysis. This integrated setup could retrieve a data set comprising analyte concentrations and associated glycan profiles in relevant biological samples, which may eventually improve early disease detection and monitoring. Prostate-specific antigen (PSA), a glycoprotein secreted by prostate epithelial cells, serves as our proof-of-concept analyte. Our platform allows multiplex targeting of PSA multiplex glycosylation profiles of PSA at "gray zone" concentrations for prostate cancer diagnosis. We additionally show the use of SERS for glycan analysis in PSA secreted from prostate cancer cell lines after androgen-based treatment. Differences in PSA glycan profiles from resistant cell lines after androgen-based treatment may eventually improve cancer treatment.

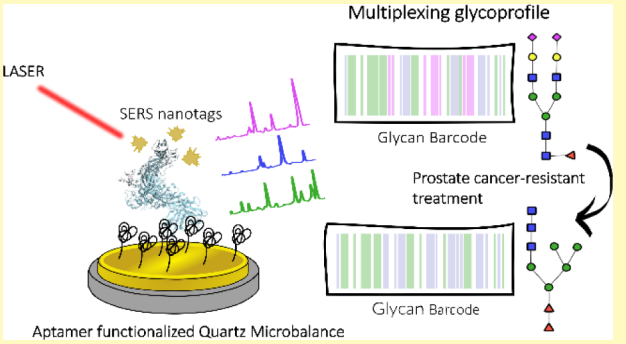

KEYWORDS: *SERS, QCM-D, glycosylation, prostate cancer, PSA*

Glycosylation is a vital process in biology, whereby the side chains of biomolecules, typically proteins and lipids, are modified with carbohydrates, significantly affecting their biological functions. Nearly half of all eukaryotic proteins undergo glycosylation, with glycoproteins commonly found in human serum taking the lead at around 70%.[1] The distinctive aspect of glycosylation lies in its remarkable complexity, which stems from the complex enzyme machinery governing glycan synthesis.[2] These enzymes are susceptible to environmental factors like pH levels, ionic strength, hormonal signals, and distant intercellular interactions. Such a sensitivity to external conditions has significant implications, particularly in disease diagnosis and monitoring.[3,4] Glycan profiles often differ between healthy and diseased cells, rendering glycans valuable biomarkers. Analysis of these profiles offers insights into disease presence, progression, and type, with a strong focus on conditions like cancer, where detection of glycan alterations can facilitate early diagnosis and tailored treatment strategies.[5]

Enzyme-linked immunosorbent assay (ELISA) is commonly used to detect glycoprotein biomarkers in clinical diagnosis.[6] However, ELISA relies heavily on specific antibodies, which are prone to suffer from low stability and reproducibility.[7,8] Therefore, alternative diagnostic tools have been developed, such as electrochemical impedance or quartz-crystal microbalance with dissipation (QCM-D).[9]

Conversely, traditional glycoprofiling methods involve releasing glycans from biomolecules and quantifying them, usually through capillary electrophoresis and liquid chromatography, often combined with mass spectrometry.[10] These

Received: May 23, 2024
Revised: August 5, 2024
Accepted: August 8, 2024
Published: August 30, 2024

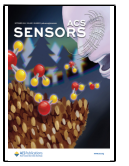

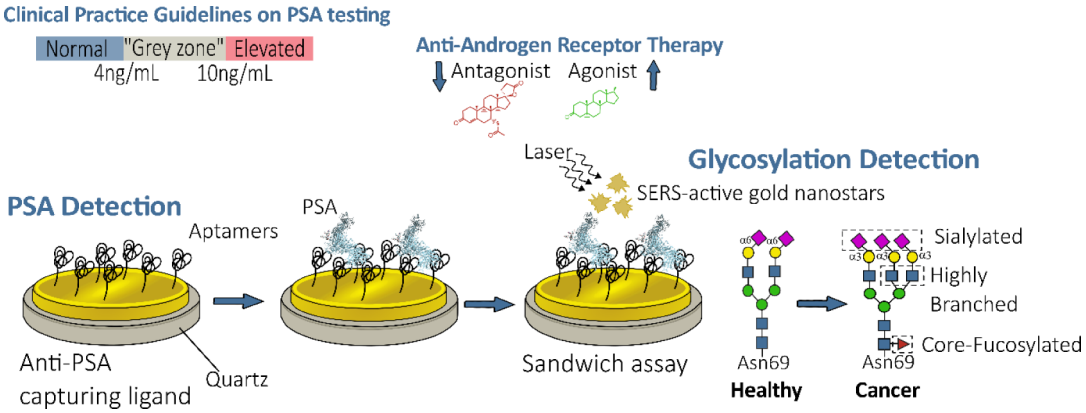

Figure 1. Schematic representation of the proposed diagnostic platform. A gold-covered QCM-D electrode is first functionalized with a PSA-specific aptamer, to determine protein concentration through frequency changes. After capturing PSA, the system is incubated with lectin-functionalized gold nanostars, which recognize PSA glycosylation, so that the glycan content is indirectly determined through relative SERS intensities.

methods are however time-consuming, require specialized equipment and personnel, and often do not provide information about glycan isomers. An alternative glycoprofiling approach utilizes lectins—proteins that selectively recognize specific glycan epitopes – in combination with transduction methods, typically based on fluorescent probes.[11,12] Therefore, accurate detection of glycosylated cancer biomarkers in the clinically relevant ranges requires novel approaches for the quantification of biomarker concentrations, together with the corresponding glycosylation profile.

Our proposed solution addresses these clinical challenges by combining two powerful tools; QCM-D and surface-enhanced Raman scattering (SERS) in a sandwich configuration approach (Figure 1), which are known to provide complementary sensing capabilities.[13] QCM-D, based on the piezoelectric effect of a quartz crystal, offers real-time, label-free detection of molecular binding events, with a remarkable sensitivity to changes in areal mass densities, as low as 1 ng/cm^2.[14] Additionally, the QCM-D electrode can be produced with various metallic coatings, including gold, which facilitates the implementation of aptamers as capture probes. Nucleic acid aptamers are single-stranded oligonucleotides (with a length of 10−100 nucleotides), which fold into well-defined three-dimensional structures that recognize and bind onto specific targets with high affinity and selectivity.[15,16] Due to their nucleic acid nature, they lack glycosylation, thus avoiding the cross-reaction and false recognition frequently occurring with standard biorecognition macromolecules (lectins and antibodies). For glycoprofiling, we use an indirect SERS-based method that provides amplified glycan detection.[17] This double sensing approach aims at the capture and quantification of biomarkers at low concentrations through aptamer-modified QCM-D surfaces, while providing information on glycosylation patterns by multiplex SERS detection. As a proof-of-concept target, we focused on the prostate-specific antigen (PSA), the most widely used biomarker for prostate cancer screening (Figure 1).

In the diagnosis of prostate cancer, men with a PSA concentration in blood between 4 and 10 ng/mL face a diagnostic "gray zone", with a 25% chance of developing prostate cancer.[18] In these cases, invasive techniques such as biopsies are needed for differential diagnosis. We propose that this diagnostic challenge can be addressed by incorporating complementary glycan profiling to enhance the assay's precision and improve early diagnosis. Evaluation of the PSA glycosylation ratio may provide the complete information required for a more reliable diagnostic tool, compared to currently available technologies for PSA detection (see Table S1).[19] Additionally, alterations to specific glycan structures have been recognized as a universal feature of malignant transformation and tumor progression. Changes in fucosylation pathways have a major influence on core fucosylation levels, which correlate with poor prognosis;[20] for example, decreased concentrations of triantennary trigalactosylated glycans and increased tetra-sialylated core-fucosylated glycans have been reported to increase the risk of a metastatic outcome.[21] Therefore, the determination of glycosylation changes in cancer biomarkers may find application in early diagnosis.[22]

In our focus on PSA modifications, we note that recent studies have revealed that glycosylation is an androgen-regulated process in prostate cancer cells. This connection reflects the interplay between hormonal regulation and molecular processes in cancer development. We thus extended our study to investigate PSA secreted from prostate cancer cell lines, under agonist/antagonist treatment. The examination of glycans in such samples offers a novel perspective on cases of resistant prostate cancer. Understanding the glycan profile, particularly under agonist/antagonist treatment, may impact diagnostic and therapeutic strategies.[23,24]

MATERIALS AND METHODS

Materials. Hydrogen tetrachloroaurate trihydrate ($HAuCl_4 \cdot 3H_2O$, ≥99.9%), silver nitrate ($AgNO_3$, ≥99.9%), L-ascorbic acid (AA, ≥99%), sodium borohydride ($NaBH_4$, 99%), 6-mercaptohexanol (MHC, 99%) and 2-mercaptoethyl ether acetic acid (HS-PEG-COOH, MW 5000 g/mol) were all purchased from Sigma-Aldrich. 4-nitrothiophenol (NTP), 2-naphthalenethiol (2-NAT), biphenyl-4-thiol (BPT), and bovine serum albumin (BSA) were purchased from Aldrich. DMEM, fetal bovine serum (FBS), penicillin-streptomycin (PS), and Coomassie (Bradford) Protein Assay were purchased from ThermoFisher. Native human prostate specific antigen protein was purchased from Abcam. Lectins *Aleuria aurantia lectin* (AAL), *Erythrina cristagalli agglutinin* (ECA) and *Sambucus nigra agglutinin* (SNA) were purchased from Vector Laboratories. 5α-Androstan-17β-ol-3-one (DHT) and spironolactone were purchased from Merk. Biotinylated and thiolated PSA aptamers were purchased from Integrated DNA Technologies (IDT) AS 5702 silicone was purchased at Advanced Proser S. L. (APS Adhesive Experts). Milli-Q water was used in all experiments, and in the case of aptamer manipulation,

https://doi.org/10.1021/acssensors.4c01252
ACS Sens. 2024, 9, 4811−4821

Milli-Q DNase and RNase-free water were used for the stock. Subsequent stock solutions were made by using autoclaved tips and Eppendorf tubes.

Preparation of Glycan-Targeting SERS Nanotags. Gold nanostars were prepared via a surfactant-free method,[25] with modifications that facilitate surface functionalization. Briefly, 20 μL of 0.128 M $HAuCl_4$ and 20 μL of 1 M HCl were added to 10 mL of deionized water under moderate stirring. After 1 min, 100 μL of 15 nm gold seed dispersion (= 0.5 mM, $Extinction_{400\ nm}$ = 1.2), prepared by citrate reduction, was added. After 20 s, 100 μL of 12 mM $AgNO_3$ and 100 μL of 50 mM ascorbic acid were added. The reaction was allowed to proceed for 3 min, and then 1 mL of 1 mM mercaptoethyl ether acetic acid (HS-PEG-COOH) was added under vigorous stirring for 30 min. After that, 10 μL of an ethanol solution of 10 mM Raman reporter (BPT, NTP, or 2NAT) was added and stirring was maintained for 30 min. Finally, AuNSs were washed by centrifugation (1192 g, 10 min).[26] Subsequently, 300 μg of each lectin (AAL, ECA and SNA, in HEPES buffer) and 1 mg of BSA (in 1× PBS) were incubated overnight at 4 °C with the AuNS dispersion. Finally, AuNSs were washed by centrifugation and stored in 1× PBS filtered buffer for further use.

To characterize the size and shape of Au NSs, transmission electron microscopy (TEM) images were collected with a JEOL JM1400 PLUS TEM operating at 120 kV, using carbon-coated 400 square mesh copper grids. UV−vis extinction spectra were obtained using an Agilent 8453 UV−vis diode array spectrophotometer to monitor the functionalization of AuNSs. The zeta potential of pegylated AuNSs, after functionalization with the Raman reporter and protein (lectin or BSA) in 1× PBS, was monitored using a zeta potential analyzer (Malvern Zetasizer Ultra). Bradford assay (Thermofisher) was used to determine the protein content following the manufacturer's instructions.

Preparation of the QCM Sensor Surface. For QCM-D measurements, we used a Q-sense E4 instrument and gold-polystyrene-coated QSX 301 sensors (14 mm diameter, 0.3 mm thickness, 5 MHz resonance frequency) purchased from Biolin Scientific. Frequency shifts of seven harmonics were recorded simultaneously: 5 MHz (1st harmonic), which is the fundamental frequency, 15 MHz (3rd harmonic), 25 MHz (5th harmonic), 35 MHz (7th harmonic), 45 MHz (9th harmonic), 55 MHz (11th harmonic), and 65 MHz (13th harmonic). All data presented in this work are the averages from of data points recorded over 1 min (1−2 s average acquisition rate), for at least three different harmonics, unless otherwise stated. Before each experiment, all QCM-D electrodes were cleaned by soaking them in piranha solution for 15 min and then washed with filtered Milli-Q water and ethanol. Each electrode was then dried under nitrogen atmosphere.

Two biofunctional surfaces were employed to test their performance as a competent biosensor for the PSA antigen. For the first surface functionalization, the QCM-D gold electrodes were coated with a self-assembled monolayer (SAM) by immersing overnight the sensors in a 1:4 mixture of ethanol solution of MHC and 1 mM of the biotin-alkylthiol HS-$(CH_2)_{11}$-EG_3-biotin, followed by rinsing with ethanol and drying under nitrogen. After being mounted in the QCM-D cell (QFM 401), the frequency shift and energy dissipation were allowed to equilibrate for at least 20 min in 1× filtered PBS, thus establishing a stable starting point. All subsequent solutions were added in continuous flow, at a flow rate of 50 μL/min, starting with a 1 mL solution of 20 μg/mL of streptavidin in 1× filtered PBS, until the frequency and dissipation curves were stabilized. A 1 mL solution of 400 nM PSA aptamer was then added and kept until stabilization. Each solution was incubated for 3 h with the QCM-D surface and washed for 30 min with 1× filtered PBS before adding the following solution. For the second surface modification, a systematic study was first performed with a long aliphatic chain (11-mercaptoundecyl)-hexa(ethylene glycol) (MUHEG), as a substitute for the PSA aptamer. Increasing MUHEG concentrations (25, 50, 100, and 200 μM) were added with the same concentration of MHC to study the organization of the final monolayer and its stability after the washing step. With the chosen experimental conditions, the electrodes were mounted in the QCM-D cell (QFM 401) and coated with a SAM, by adding (at a flow rate of 20 μL/min) a 1 mL mixture of 25 μM MHC and 5 μM of the thiolated PSA aptamer. After stabilization of frequency and dissipation, and incubation for 3 h, the electrodes were washed for 30 min with 1× filtered PBS.

QCM Measurements. All QCM-D measurements were carried out on a Q-Sense E4 instrument (Biolin Scientific, Sweden). Frequency and dissipation response were analyzed using the Qtools software. Considering the properties inherent to the two layers formed within the experimental setups, the streptavidin (SA) layer and the PSA aptamer layer, a conventional Sauerbrey model was employed to evaluate the SA layer. However, deposition of the aptamer creates a more hydrated layer, causing damping of the QCM-D electrode oscillation. A more sophisticated Voight viscoelastic model,[27] which also considers dissipation (ratio between lost and stored energy from the system during one oscillation cycle), allowed for a more precise calculation and accurate determination of mass variations, considering the decrease in frequency and increase in dissipation.

PSA Detection. In each of the biofunctional surfaces, a competent biosensor for the PSA antigen was tested by addition (at continuous flow rates of 50 μL/min and 20 μL/min, for the streptavidin/biotinylated aptamer and the thiolated aptamer, respectively) of a 40 nM solution of pure PSA antigen in 1× filtered PBS. After stabilization, it was incubated for 3 h and then washed for at least 30 min with 1× filtered PBS. To determine the sensitivity toward PSA in more complex media, four solutions of 40 nM PSA were mixed with 0, 25, 50, and 75% BSA, and added under the same conditions as detailed above. For the detection of PSA in human cancer cell lines after treatment with an agonist or antagonist of the androgen receptor, each supernatant was centrifuged at 1000*g* for 5 min to discard cells, and then concentrated with Amicon Ultra 15 mL 10K centrifugal filter (Merck) in 1× filtered PBS. 500 μL was added in continuous flow (flow rate 50 μL/min), incubated for 3 h, and then washed with 1× filtered PBS until stabilization of frequency and dissipation.

SERS Sandwich Glycan Profile Determination. For the determination of the glycosylation pattern of the PSA antigen, 100 μL of a mixture of the three Raman reporters NTP, BPT, and 2NAT in 1× filtered PBS (at 0.1 mM [Au]) was added in continuous flow to the QCM-D cells. It was then incubated for 30 and washed by adding 1× filtered PBS in continuous flow (20 μL/min) for 15 min. QCM-D electrodes were then unmounted from the cells, dried under a nitrogen atmosphere, and stored at 4 °C until use.

Glycoprotein Array. To ensure the affinity of the lectin-functionalized gold nanoparticles for their specific glycans, a glycoprotein array was prepared. Glass slides covered with active *N*-hydroxysuccinimide (NHS) hydrogel (NEXTERION Slide H, Schott) were used to immobilize several glycoproteins. To facilitate incubations and washes, a multiheaded 3D Discovery bioprinter (RegenHU, Switzerland) was used to print silicone wells. A transparent silicone adhesive AS 5702 (ACC silicones Europe) was extruded using a pneumatic pressure-driven cartridge at 0.2 MPa and a conical plastic needle with an inner diameter of 0.20 mm and 10 mm/s printing speed. The G-code was produced using BIOCAD software (RegenHU, Switzerland) to produce wells with 5 mm diameter and 4 mm height. The printed objects were allowed to harden at room temperature for 24 h prior to use.

20 μL of 1.5 mg/mL fetuin and asialofetuin and 20 μL of 1 mg/mL mucin solutions were incubated overnight at 4 °C in PBS containing 0.01% Tween-20. Subsequently, excess liquid was removed, and the remaining NHS-free groups were deactivated by incubating with 20 μL of ethanolamine (50 mM) in sodium borate buffer (50 mM at 4 °C) for 1 h. Each well was then washed with PBS containing 0.01% Tween-20 and dried. Finally, 20 μL of 1 mM [Au] lectin-functionalized AuNSs was incubated in each well for 30 min, washed with PBS containing 0.01% Tween-20 and air-dried.

Cell Culture. PC3 (androgen-independent human prostatic small cell carcinoma) and LnCaP (androgen-sensitive human prostate adenocarcinoma) cells were grown in Dulbecco's modified Eagle

https://doi.org/10.1021/acssensors.4c01252
ACS Sens. 2024, 9, 4811−4821

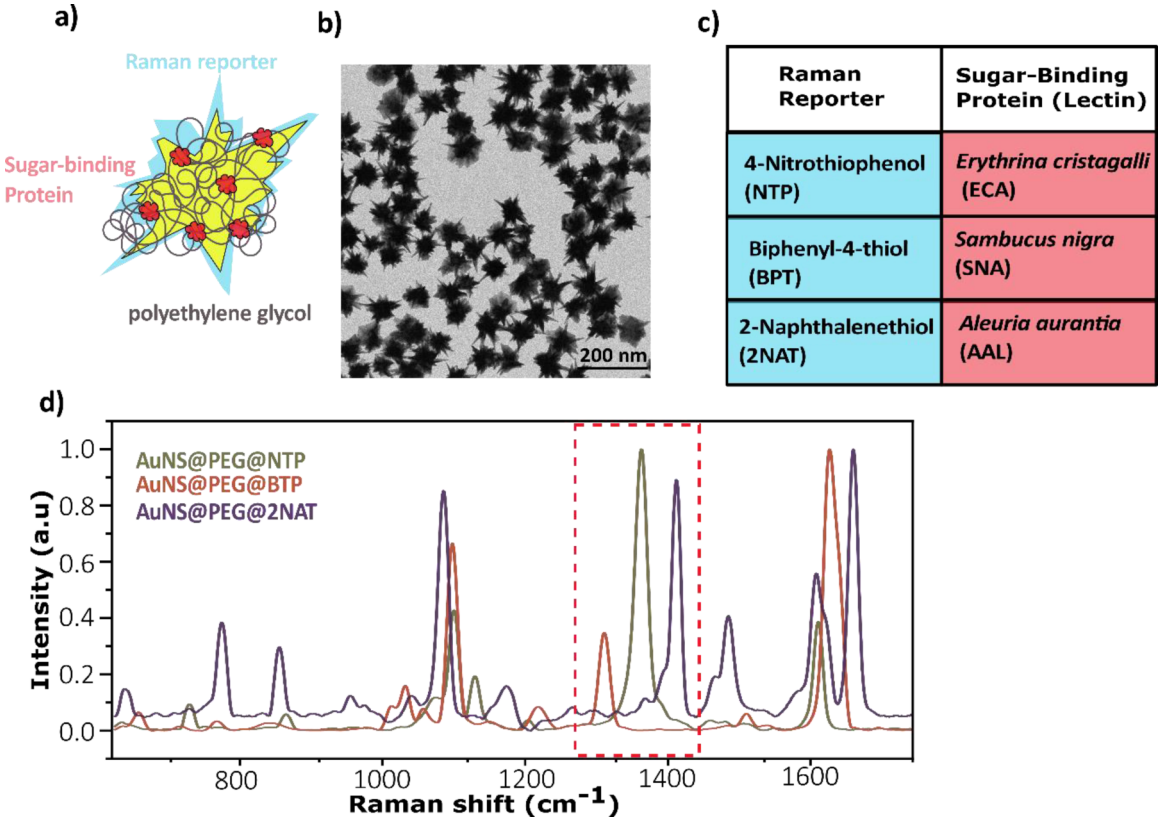

Figure 2. Characterization of lectin-SERS nanotags. (a) Schematic representation of PEGylated gold nanostars functionalized with a characteristic Raman reporter and a sugar-binding protein (lectin). (b) Representative TEM image of freshly prepared PEGylated gold nanostars. (c) Table listing the different RaR/lectin pairs. (d) Representative SERS spectra for each AuNS@RaR: BPT (orange), NTP (green), and 2NAT (purple), normalized to 1 for the maximum peak intensity. Framed in red is one representative peak for each RaR, selected for multiplexing SERS measurements: 1280 cm^{-1} for BPT, 1342 cm^{-1} for NTP, and 1380 cm^{-1} for 2NAT.

media (DMEM) and Roswell Park Memorial Institute (RPMI) 1640, respectively, with 10% fetal bovine serum (FBS) and 1% penicillin-streptomycin. Cells were detached for passages or investigations when they reached 80% confluence. Flasks containing LnCaP cells were pretreated with poly-L-lysine to enhance cell adherence. In all the drug supplementation assays, the cells were harvested in 12-well plates at 10^5 cells/mL in 1 mL DMEM or RPMI. Then, the cells were exposed to the selected drugs: 125 nM 5α-androstan-17β-ol-3-one (DHT) or 125 nM spironolactone, beyond the initial 24 h of cell seeding. After 72 h of supplementation, supernatants were collected for further examination.

SERS Measurements. SERS spectra were recorded using an InVia Reflex Raman microscope (Renishaw plc), including an optical microscope (Leica) with an XYZ scanning stage coupled to a high-throughput Raman spectrometer equipped with a 1024 × 512 front-illuminated CCD (charged coupled device) detector and a grating of 1200 grooves mm^{-1} for the 785 nm laser. SERS maps of 10 × 10 points were recorded with an L50× objective, an integration time of 2s, and 8.6 mW laser power. For measurements on the QCM-D electrode surface, the average of 10 maps was used to generate SERS spectra, using Renishaw's WiRE software in every experiment; in the case of the glycoprotein array, the average was obtained with 5 maps per well.

PLS Regression. We employed Partial Least Squares Regression (PLSR), utilizing the Scikit-learn library in Python, to develop a multivariate regression model. This model estimates the contribution of each SERS tag (NTP, BTP, and 2-NAT) to the final spectra. Our calibration data set comprised 300 spectra, representing 25 different conditions with varying concentrations of all three components. These conditions included pure samples for acquiring spectra of each component in isolation, balanced samples with equal proportions of all three components, and randomly proportionated samples where the concentration of each component was varied arbitrarily. To construct the PLS calibration model, we used four latent variables and selected a subset of significant variables. This selection was optimized to achieve the lowest root-mean-square error (RMSE) with respect to the training data. The model's accuracy was subsequently evaluated on a test set, resulting in RMSE values of 7.94, 6.27, and 8.65 for NTP, BTP, and 2-NAT predictions, respectively (Figure S1). Ultimately, this regression model was applied to approximate alterations in PSA glycosylation patterns following cellular exposure to the specified agonist.

RESULTS AND DISCUSSION

Preparation of Glycan-Targeting SERS Nanotags. SERS can be used to detect a specific target through recognition molecules adsorbed on so-called SERS nanotags as labels.[28] Our SERS nanotags comprise Au nanostars (Au NSs), with a localized surface plasmon resonance (LSPR) around 785 nm, and an outer layer made of lectins for both nanotag stabilization and PSA glycosylation recognition (Figure 2a). To investigate the carbohydrate composition (glycosylation) of PSA, three different lectin proteins were incorporated on different nanotags, namely: *Erythrina cristagalli agglutinin* (ECA), which recognizes the terminal galactosylated structure, specifically the Galβ1−4GlcNAc disaccharides;[29] *Sambucus nigra agglutinin* (SNA), specific against terminal α2,6-linked sialic acid residues;[30] and *Aleuria aurantia lectin* (AAL), which binds to fucosylated oligosaccharides.[29,31] As detailed in the experimental section, the synthesis of AuNSs was optimized to match the LSPR

https://doi.org/10.1021/acssensors.4c01252
ACS Sens. 2024, 9, 4811−4821

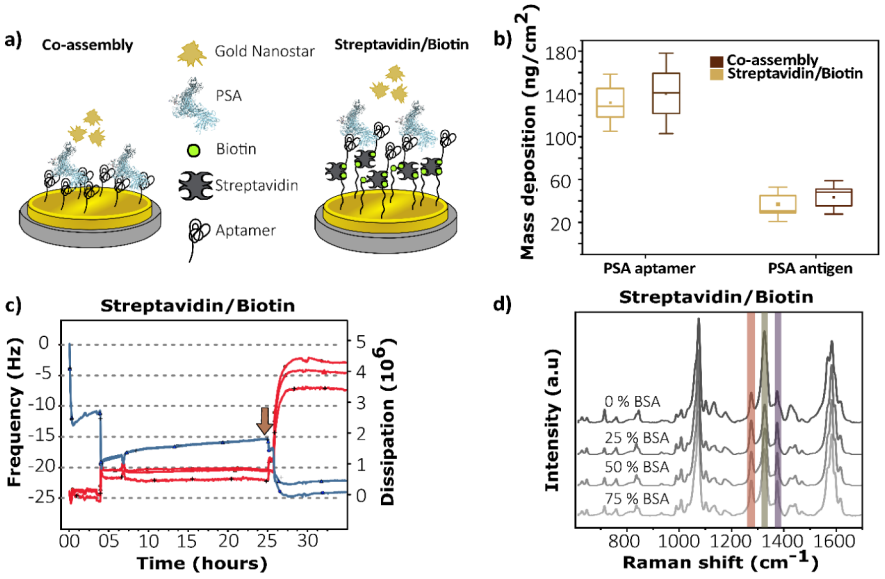

Figure 3. Characterization of the QCM-D-based PSA biosensor. (a) Schematic representation of the two types of biofunctional surfaces tested for the PSA biosensor: a thiolate/aptamer coassembly model (left) and a streptavidin/biotinylated aptamer model (right). (b) Plot of PSA aptamer mass deposition (ng/cm^2) and detection of PSA antigen (from a 40 nM solution in water), for each model, as labeled. (c) Time course of frequency (blue) and dissipation (red) during assembly in the streptavidin/biotin model. The arrows mark the addition of 40 nM PSA antigen solution. (d) Average SERS spectra recorded from the QCM-D electrode after addition of PSA antigen solution spiked with 0%, 25%, 50%, and 75% BSA. The characteristic peaks for each RaR are color coded: BPT (orange), NTP (green), and 2NAT (purple). SERS measurements were recorded with a L50× objective, 2 s integration time of a 785 nm laser, 8.6 mW power at the surface.

maximum with the Raman laser excitation wavelength at 785 nm. AuNSs comprising a central core (51.7 ± 7.9 nm in diameter) and multiple spikes with an average core-to-tip length of 17 nm (Figure 2b) were first functionalized with thiolated polyethylene glycol (AuNS@PEG).[26] After PEGylation, different thiolated Raman reporters (RaR), 4-biphenylthiol (BPT), 2-naphthalenethiol (2NAT), or 4-nitrothiophenol (NTP), were attached onto the AuNS surface, leading to an LSPR redshift, from 736 to 789 nm (Figure S2). After RaR functionalization, protein conjugation was carried out by physisorption of lectins, as previously reported for targeted sensing nanoprobes.[32,33] For multiplex analysis, each AuNS@RaR was functionalized with a different lectin (SNA, ECA, or AAL), thereby generating three different glycan-targeting nanotags: BPT-AuNS@SNA, NTP-AuNS@ECA, and 2NAT-AuNS@AAL (Figure 2c). The stability of the probes was monitored by UV−vis spectroscopy for 24 h (Figure S3). Protein adsorption was evaluated through Zeta potential measurements (Figure S2) and quantified using the Bradford assay. The RaR/lectin pairs, BPT-AuNS@SNA, NTP-AuNS@ECA, and 2NAT-AuNS@AAL, exhibited changes in Zeta potential from −27.6 ± 0.8 to −20.5 ± 1.2 mV; from −32.3 ± 1.8 to −19.6 ± 1.4 mV, and from +13.8 ± 1.1 to −14.4 ± 1.1 mV, respectively, suggesting successful lectin functionalization. All lectin SERS nanotags exhibited a similar negative net charge, which is consistent with previously reported Zeta potential values for protein−AuNP conjugates.[34] Bradford assay was applied to quantify the amount of protein adsorbed on the Au NS surface, by indirectly measuring the amount of lectin in the supernatant after optimized adsorption. The results indicated depositions of 73−87% (with respect to the initial amount of lectin, Table S2). Higher lectin/AuNS ratios did not result in higher amounts of immobilized lectins.

The SERS performance of each AuNS@lectin nanotag was evaluated individually after functionalization (Figure S4). Table S3 summarizes the characteristic Raman peaks and assigned vibrations for all three RaRs. In the context of multiplex detection, we ultimately selected the most intense peaks within each SERS fingerprint that can be readily distinguished in mixtures comprising all three SERS nanotags, namely: 1280 cm^{-1}, 1342 cm^{-1}, and 1380 cm^{-1}, for BPT, NTP, and 2NAT, respectively (Figure 2d). Apart from single peak selection, we built a Partial Least Squares (PLS) calibration model to correlate entire spectra with the ratios between nanotags (see Materials and Methods).

Tandem SERS/QCM-D Detection of Glycosylated PSA. QCM-D measurements were initially used to monitor the assembly of PSA aptamers onto biofunctionalized quartz substrates. Two different strategies were employed, one based on thiol-gold chemistry (coassembly model) and another through biotin−streptavidin interactions (Figure 3). In QCM-D, a real-time piezoelectric sensor provides information on the amount of mass binding onto the gold-covered quartz crystal, as well as changes of viscoelastic properties over time.[35] Both strategies were optimized to enhance the interaction between the PSA aptamer and its protein target (Figure 3a). We first optimized the parameters potentially affecting the coverage of the PSA aptamer, i.e., flow conditions (μL/min), incubation periods, and washing steps.

In the thiol−gold chemistry model, an aliphatic thiol was introduced to stabilize the orientation of the PSA aptamer layer on the gold surface.[36,37] This process was fine-tuned through a systematic study using MUHEG, to ensure optimal conditions to form a self-assembled monolayer (Figure S5). The experiments with the coassembly biosurface once the PSA aptamer was included (see Materials and Methods for details) resulted in a decrease in QCM frequency, indicating the adsorption of thiolated molecules on the gold electrode. The observed stabilization period (about 15 min) was consistent with the formation of a monolayer (Figure S6). Quantitatively,

https://doi.org/10.1021/acssensors.4c01252
ACS Sens. 2024, 9, 4811−4821

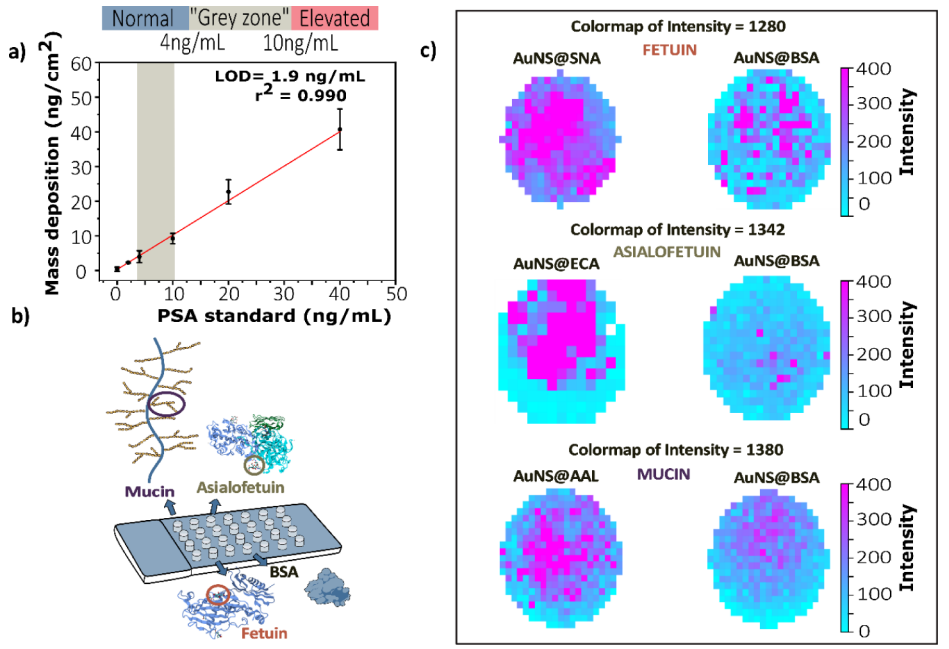

Figure 4. (a) Calibration curve for the detection of commercial PSA from seminal fluid in PBS buffer. Each point is the average of three different harmonics from three simultaneous measurements. The definition of PSA clinical ranges is shown for clarity. (b) Determination of the affinity of lectin-covered SERS nanotags for their specific glycans. Scheme of a glycoprotein array with a specific glycoprotein for each AuNS@RaR@Lectin and AuNS@RaR@BSA as a negative control. (c) SERS maps for individual wells from glycoprotein arrays, treated with a selective lectin-SERS nanotag for BPT (SNA lectin), NTP (ECA lectin), and 2NAT (AAL lectin), together with BSA negative controls. SERS measurements were recorded with a L50× objective, integration time of 2 s and 8.6 mW power of a 785 nm laser.

for a deposition of 131.8 ± 26.7 ng/cm^2 PSA aptamer (after subtracting the mass of MHC), we determined an average of 45.6 ± 11.3 ng/cm^2 of PSA antigen deposited onto the QCM-D electrode surface (Figure 3b, coassembly model).

For the biotin−streptavidin model, by increasing the streptavidin surface density from 100 to 400 ng/cm^2, a 4-fold increase in PSA aptamer deposition was achieved, reaching a value of 123.9 ± 15.9 ng/cm^2 (Figure 3b). This result is comparable to that for the coassembly model when a biotinylated PSA aptamer was used, which indicates reliable PSA antigen detection and facilitates direct comparison between both models. This model additionally demonstrated better reproducibility, with PSA antigen deposition of 36.9 ± 1.6 ng/cm^2, comparable to the coassembly model (45.6 ± 11.3 ng/cm^2 of PSA). The lower dissipation observed in the coassembly model suggests the formation of a more rigid film compared to the biotin−streptavidin model.

These results can be explained as follows: the isoelectric point of PSA falls within the range between 6.9 and 7.2.[38] Consequently, its interaction with the PSA aptamer introduces a subtle increase in negative charge to the biosensor surface, mainly when operated at pH 7.0−7.4 (PBS buffer). The binding of PSA onto the PSA aptamer additionally triggers a conformational change, causing the aptamer structure to change from a single-chain into a complex and stable chain structure.[39] This transformation amplifies the charge density on the aptamer and expands its geometrical area, thereby facilitating[40,41] the approach of other molecules to the surface during the binding process.[27] Therefore, the distance between the QCM-D electrode surface and the newly formed protein layer is significantly reduced in the coassembly model, producing a more rigid and compact layer (Figure S6). Whereas the biotin−streptavidin model allows more free space between the PSA layer and the QCM-D electrode, evident in the dissipation patterns registered during the addition of PSA antigen (Figure 3c). The biotin−streptavidin model displays a more viscoelastic behavior, with higher ΔD,[42] around 4×10^6 (Figure 3c) At the same time, ΔD decreases to a situation comparable to a Sauerbrey model (see Materials and Methods) in the coassembly model, with ΔD around 0.5×10^6 (Figure S6).[43] With a better understanding of the distinct structural and dynamic characteristics of both models, we set to analyze their sensitivity for PSA recognition.

We then tested the antifouling capabilities of each biosurface, by incubating them with a 40 nM PSA antigen solution. Then, either SNA lectin-functionalized or BSA-functionalized (negative control) AuNS were added, and their adsorption was studied by scanning electron microscopy (SEM). SEM images (Figure S7) revealed negligible adhesion of BSA-functionalized AuNs, but significant deposition of lectin-functionalized AuNSs, in agreement with a specific binding of AuNSs that carry a lectin recognizing PSA antigen glycans on the QCM-D electrode surface. These results were confirmed by SERS mapping, showing high SERS intensity throughout the surface for lectin-functionalized AuNS, but negligible signal in the maps obtained with BSA-functionalized AuNS (Figure S8). Incidentally, in the control (BSA-funcionalized AuNSs), SERS signal was only appreciated in the area outside the biofunctional surface, i.e., on the rough edges of the electrode.[44,45]

We next studied the antifouling efficacy of both biosurfaces, in the presence of increasing concentrations of bovine serum albumin (BSA), up to the typical concentration in serum (60%). For the coassembly model, we observed a decrease in frequency when exposed to increasing amounts of BSA, which is indicative of strong unspecific interactions (deposited mass: 462.0 ± 12.6 ng/cm^2, 336.6 ± 2.5 ng/cm^2, and 323.2 ± 3.0 ng/cm^2, for 25, 50, and 75% BSA concentrations, respectively,

https://doi.org/10.1021/acssensors.4c01252
ACS Sens. 2024, 9, 4811−4821

see Figure S9). We thus concluded that the coassembly biosurface exhibited poor antifouling properties. On the other hand, the biotin−streptavidin model exhibited robust antifouling properties, maintaining consistent results even when exposed to higher concentrations of BSA, with an average deposited mass of 27.5 ± 1.6 ng/cm^2, in the same range as the value of 36.9 ± 1.6 ng/cm^2 obtained with PSA buffer (Figure S10).

Ultimately, glycan profile characterization and PSA detection were performed in tandem by QCM-D monitoring and subsequent SERS measurements. Lectin-coated SERS nanotags were added and compared with the known spectra of a 1:1:1 mixture of SERS nanotags (Figure S11), as described in the Materials and Methods section. SERS spectra were then recorded from the QCM-D electrodes (Figures 3d and S12), which confirmed the differences in antifouling efficiency. In the thiol-gold chemistry model, the SERS signal specific to surface glycans (corresponding to 2NAT; peak at 1380 cm^{-1}), exhibited a decrease in intensity as BSA concentration was increased, while a new peak at 1390 cm^{-1} increased at the same rate (Figure S12). This suggested that the interaction between lectin-functionalized AuNS and surface glycans was affected by the biosurface response to BSA, in agreement with the poor antifouling character of the coassembly model. Conversely, the SERS data for the biotin−streptavidin model retained the intensity of the characteristic peaks for all the lectin-covered nanotags, even under conditions approaching clinical sample complexity. The signal corresponding to 2NAT at 1380 cm^{-1} remained stable across different BSA concentrations, indicating that nonspecific interactions did not compromise the interactions with lectin-functionalized AuNS (Figure 3d).

Given the superior properties of the biotin−streptavidin model in terms of antifouling, consistent detection results, and preserved SERS signal quality, we selected this model for further experiments, thus discarding the coassembly model.

Sensitivity and Specificity. One of the main objectives of the dual sensor is to distinguish potential cancer-related events from other confounding factors, such as inflammation, particularly in the clinical range referred to as the "gray zone" in prostate cancer. This diagnostic challenge required a critical assessment of the sensor's sensitivity within the context of clinical diagnosis. To assess the sensitivity of the QCM-D biosurface platform for PSA detection, a series of assays were conducted on a commercial PSA solution in PBS buffer. We started from the highest PSA concentration of 40 ng/mL (Figure 4a), mirroring the diagnosis of an aggressive prostate cancer, which was found to produce significant alterations in both Δf and ΔD, indicating substantial PSA binding onto the biosurface. We then transitioned toward clinically relevant PSA levels for prostate cancer diagnosis and monitoring. We thus lowered the commercial antigen concentration to 20, 10, 4, and 2 ng/mL, effectively capturing the concentrations characteristic of the clinical "gray zone". The sensitivity of the biosensor was still sufficient at these lower concentrations, as shown by meaningful shifts in both Δf and ΔD. The resulting mass bindings were calculated to be 22.7 ± 3.5 ng/cm^2, 8.3 ± 1.2 ng/cm^2, 4.7 ± 0.1 ng/cm^2 and 2.3 ± 0.6 ng/cm^2, for PSA concentrations of 20, 10, 4, and 2 ng/mL, respectively. These data confirm the feasibility to detect varying levels of PSA concentration using QCM-D. The working concentrations employed by the QCM-D platform toward PSA in buffer were derived from 3 independent experiments, obtaining a limit of detection (LOD) of 1.9 ng/mL, i.e., within the healthy patient zone (Figure 4a). For clarification, we define the LOD as the minimum concentration of the analyte that can be detected by the sensor, calculated from the standard deviation of the blank and the slope of the calibration curve.[27,46−48] Blank measurements were performed by adding PBS buffer to the biosurfaces and recording the response of frequency and dissipation.

A control experiment was additionally conducted to ensure that lectins adsorbed on AuNSs could effectively recognize carbohydrates. A model glycoprotein array was employed to visualize the interaction of lectin SERS nanotags with their specific glycans (Figure 4b,c). Three glycoproteins−fetuin, asialofetuin, and porcine mucin−were covalently immobilized on microarray glass. The glycoprotein surfaces were then incubated with SERS nanotags functionalized with the appropriate lectin, to bind onto the glycoprotein surface. In parallel, AuNSs functionalized with BSA were employed as a negative control (see scheme in Figure 4b). A comparative analysis of spatial distributions and signal intensities was performed for sugar-binding (lectin-functionalized) AuNS and those derived from the negative, nonspecific (BSA-functionalized) AuNS controls.

SERS maps were recorded for each spot in the array, offering a visual validation and valuable insights into the specificity of the interactions under investigation. These images allowed us to examine the distribution of high-intensity pixels across maps, associated with the characteristic peaks of the RaRs used for multiplexing: 1280 cm^{-1} for BPT, 1342 cm^{-1} for NTP, and 1380 cm^{-1} for 2NAT. Such high-intensity pixel distributions were prominently observed in each well subjected to incubation with lectin-functionalized AuNS. This result confirms the binding of lectin-functionalized SERS nanotags onto their target glycans (Figure 4c). Conversely, in the control experiment involving BSA-functionalized AuNSs, the observed signal was significantly less intense (Figure 4c) and limited to isolated pixels, corresponding to small clusters of unspecifically bound BSA-functionalized AuNS on the glass surface. Additionally, the signal obtained from the background (hydrogel-modified glass surface) was more prominent because of the low intensity from BSA-functionalized AuNS (Figure S13). These results are consistent with the unspecific nature of the control, because BSA-functionalized probes hardly exhibit any interaction with glycoproteins.

In summary, the average SERS spectra and maps obtained from the glycan array collectively confirm the selective binding of lectin-functionalized AuNSs onto their target glycans, while also highlighting the possibility of minor nonspecific interactions in the control experiments involving BSA-functionalized AuNSs. It is therefore important to note that PSA captured by the QCM crystal after flowing with BSA-functionalized AuNSs does not provide any appreciable signal from the SERS nanotag.

Monitoring Glycosylation Patterns on PSA Secreted from Cancer Cells. Prostate cancer is recognized as an androgen-driven tumor, where the growth and progression of cancer cells largely depend on activation of the androgen receptor pathway. Consequently, many therapeutic strategies for prostate cancer aim to disrupt this pathway.[49] We were specifically interested in tumors that do not respond to androgen suppression treatment, with a poor prognosis, and whether PSA glycosylation might be a determining aspect to be considered toward a more personalized therapy in resistant

https://doi.org/10.1021/acssensors.4c01252
ACS Sens. 2024, 9, 4811−4821

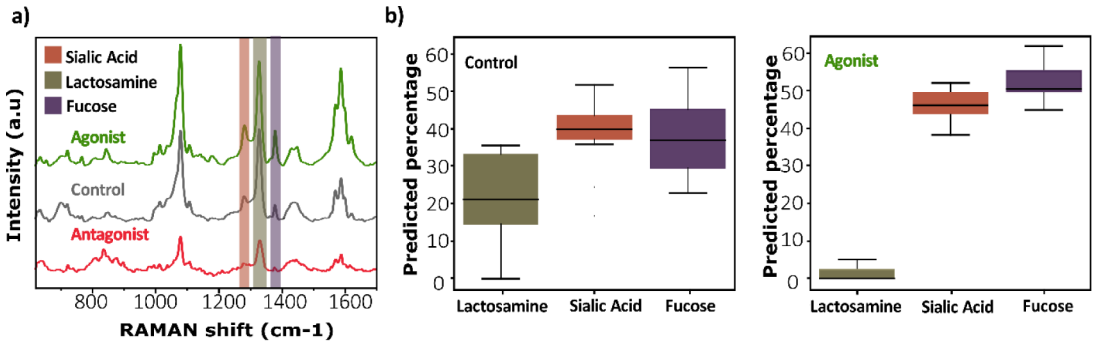

Figure 5. (a) Average SERS spectra recorded from the QCM-D electrode for the control and upon incubation with the androgen receptor agonist and antagonist. Characteristic peaks for each RaR are marked: BPT (orange), NTP (green) and 2NAT (purple). (b) Box charts of the predicted sugar percentages present in the PSA antigen surface for the control and upon incubation with the androgen receptor agonist.

prostate cancer. We thus aimed at the determination of potential changes in the glycosylation of secreted extracellular PSA, upon activation of androgen receptors in prostate cancer cells. Antagonist treatment was introduced as a control of PSA concentration-dependent detection. The dynamic evolution of secreted PSA was assessed after both agonist and antagonist treatments.

We selected two different prostate cancer human cell lines: LnCaP, sensitive to hormone treatment, and PC3, which lacks the androgen receptor.[50] The experimental process was initiated by introducing in the QCM-D sensor the supernatants from three differently treated replicates. We first measured the dynamics of PSA concentration after incubation with both agonists and antagonists of the androgen receptor, for both cell lines, to validate the expected cellular response toward each metabolite, i.e., an increase or a decrease of PSA concentration in the medium (scheme in Figure S14).

As a control, we replicated the experiment with the cell line lacking sensitivity toward the androgen receptor, PC3, to ascertain that any observed alterations would be due to interactions with the androgen receptor. The results were in accordance with our expectations. In the hormone-sensitive cell line, a substantial rise in PSA concentration within the supernatant was evident in the presence of the agonist (Figure S15). However, a slight reduction was observed in the presence of the antagonist. Conversely, the nonsensitive cell line, lacking the androgen receptor, displayed no discernible changes, with any observed variations being attributed to inherent variability in the QCM-D system itself (Figure S15). Furthermore, we implemented an additional control point to ensure the consistent and reproducible deposition of the PSA aptamer. These results emphasized the confidence that the detected PSA concentrations in each experimental condition, for both cell lines, were solely influenced by the actual concentrations in the supernatant and not by any variations in the fabrication of the biosurfaces (Figure S15).

Once the desired environmental conditions were established, we measured the SERS signal intensities for each experimental condition. The primary peaks associated with multiplexing (1280, 1342, and 1380 cm^{-1}) were readily distinguishable in the corresponding SERS spectral profiles, and their intensities correlated well with antigen concentration. Although the spectra obtained under varied experimental conditions can be initially assessed through simple visual inspection as depicted in Figure 5a, this approach falls short of the accuracy required for in-depth analysis of peak/glycosylation profiles. To address this limitation, we developed a partial least-squares (PLS) regression model that establishes a link between the entire spectra and the relative concentrations of the three Raman reporters (BPT, NTP, and 2NAT). This PLS mode, which goes beyond previous peak ratio analyses, was then applied to predict the glycosylation profiles of secreted PSA by the cells, across the different biological conditions (control vs agonist, as illustrated in Figure 5b). Specifically, there was a noticeable decrease in the contribution of lactosamine to the final spectra upon agonist treatment, dropping from 20% to residual levels. This shift contrasts, in turn, with the observed dominance of fucose and sialic related peaks.

The glycan-enhanced or reduced expression might provide new insights for accurate diagnosis of disease state including its aggressiveness, as well as information about progression and treatment effectiveness. The lectins chosen in the present study recognize epitopes that have been correlated with different stages of prostate cancer, such as fucosylation and sialylation. Besides, the output of the PLS model reflects an increase in fucosylation, a well-documented mechanism in aggressive prostate cancer types, accompanied by a slight increase in α-2,6-sialylation upon activation with androgen receptors, in agreement with literature data.[51,52] We also detected a prominent decrease in terminal lactosamine (Galβ-1,4-GlcNAc) moieties, which may indirectly provide evidence of a switch from α-2,6 to α-2,3 sialic acids, which are not recognized by the SNA lectin. Still, their presence would hinder the recognition of internal lactosamine moieties by the ECA lectin. The presence of α-2,3 sialic acids in PSA has been correlated to prostate cancer aggressiveness.

CONCLUSIONS

This study presents a multifaceted biosensing platform for the detection and characterization of glycoproteins, focusing on the prostate-specific antigen (PSA). Our approach relied on the use of lectin-covered gold nanostars as SERS functional probes (nanotags). The selection of *Sambucus nigra*, *Erythrina cristagalli*, and *Aleuria aurantia* lectins as sugar-binding proteins yielded highly specific and functional nanotags, capable of precisely recognizing their target glycans. Furthermore, we developed a sensitive and selective QCM-D surface through aptamer-based sensing, tailored for PSA detection. The devised biosurface exhibited excellent antifouling properties, ensuring reliable performance, even in the presence of interfering proteins. Our QCM-D surface demonstrated high selectivity for the PSA antigen, a crucial characteristic for reliable biomarker detection. To enhance the capabilities of our

https://doi.org/10.1021/acssensors.4c01252
ACS Sens. 2024, 9, 4811−4821

biosensing platform, we integrated the QCM-D functional surface with SERS multiplexing. This combination allowed for the simultaneous detection of multiple glycan patterns, thereby providing a comprehensive assessment of glycoproteins and a reliable multiplexing system. Our platform can detect PSA antigens within the clinically significant range known as the "gray zone," thus offering a sensitive and quantitative approach to clinical diagnostics. Coupling the QCM-D system with multiplex SERS allowed us to detect glycosylation patterns. Our work demonstrates the integration of various techniques to create a powerful platform for glycoprotein analysis. This platform holds promise for improving the accuracy of clinical diagnostics, particularly in prostate cancer screening and treatment monitoring, by providing both quantitative antigen detection and detailed glycan pattern profiling.

■ ASSOCIATED CONTENT

Supporting Information

The Supporting Information is available free of charge at https://pubs.acs.org/doi/10.1021/acssensors.4c01252.

PLS calibration, additional characterization of SERS tags, and complementary SERS and QCM-D measurements (PDF)

■ AUTHOR INFORMATION

Corresponding Authors

Isabel García − *CIC biomaGUNE, Basque Research and Technology Alliance (BRTA), Donostia-San Sebastián 20014, Spain; Biomedical Research Networking Center in Bioengineering, Biomaterials, and Nanomedicine (CIBER-BBN), Donostia-San Sebastián 20014, Spain;* Email: igarcia@cicbiomagune.es

Luis M. Liz-Marzán − *CIC biomaGUNE, Basque Research and Technology Alliance (BRTA), Donostia-San Sebastián 20014, Spain; Biomedical Research Networking Center in Bioengineering, Biomaterials, and Nanomedicine (CIBER-BBN), Donostia-San Sebastián 20014, Spain; IKERBASQUE, Basque Foundation for Science, Bilbao 48009, Spain; Cinbio, Universidade de Vigo, Vigo 36310, Spain;* orcid.org/0000-0002-6647-1353; Email: llizmarzan@cicbiomagune.es

Authors

Laura Armero − *CIC biomaGUNE, Basque Research and Technology Alliance (BRTA), Donostia-San Sebastián 20014, Spain; Department of Applied Chemistry, University of the Basque Country, Donostia-San Sebastián 20018, Spain*

Javier Plou − *CIC biomaGUNE, Basque Research and Technology Alliance (BRTA), Donostia-San Sebastián 20014, Spain; CIC nanoGUNE, Basque Research and Technology Alliance (BRTA), Donostia-San Sebastián 20018, Spain; Biomedical Research Networking Center in Bioengineering, Biomaterials, and Nanomedicine (CIBER-BBN), Donostia-San Sebastián 20014, Spain;* orcid.org/0000-0002-3298-269X

Pablo S. Valera − *CIC biomaGUNE, Basque Research and Technology Alliance (BRTA), Donostia-San Sebastián 20014, Spain; Department of Applied Chemistry, University of the Basque Country, Donostia-San Sebastián 20018, Spain; Biomedical Research Networking Center in Bioengineering, Biomaterials, and Nanomedicine (CIBER-BBN), Donostia-San Sebastián 20014, Spain; CIC bioGUNE, Basque Research and Technology Alliance (BRTA), Derio 48160, Spain*

Sonia Serna − *CIC biomaGUNE, Basque Research and Technology Alliance (BRTA), Donostia-San Sebastián 20014, Spain;* orcid.org/0000-0002-2085-4412

Complete contact information is available at: https://pubs.acs.org/10.1021/acssensors.4c01252

Funding

Funding is acknowledged from the European Research Council (ERC AdG 787 510, 4DbioSERS) and CIBER-Consorcio Centro de Investigación Biomédica en Red (CB06/01/2012), Instituto de Salud Carlos III, Ministerio de Ciencia e Innovación.

Notes

The authors declare no competing financial interest.

■ ACKNOWLEDGMENTS

The authors thank Dr. Judith Langer for assistance with SERS measurements, Dr. Clara García Astrain for assistance in the fabrication of glycoprotein array slides, and Dr. Marco Möller and the CIC biomaGUNE technological platform for assistance with scanning electron microscopy characterization.

■ ABBREVIATIONS

ELISA, enzyme-linked immunosorbent assay; QCM-D, quartz-crystal microbalance with dissipation; SERS, surface-enhanced Raman scattering; PSA, prostate-specific antigen; ER, endoplasmic reticulum; MHC, 6-mercaptohexanol; NTP, 4-nitrothiophenol; 2NAT, 2-naphthalenethiol; BPT, biphenyl-4-thiol; BSA, bovine serum albumin; DMEM, Dulbecco's modified Eagle medium; FBS, fetal bovine serum; PS, penicillin-streptomycin; AAL, *Aleuria aurantia* lectin; ECL, ECA, *Erythrina cristagalli* lectin; SNA, *Sambucus nigra* lectin; DHT, 5α-androstan-17β-ol-3-one; HEPES, 4-(2-hydroxyethyl)-1-piperazine-ethanesulfonic acid; PBS, phosphate-buffered saline; TEM, transmission electron microscopy; UV−vis, ultraviolet−visible spectroscopy; SAM, self-assembled monolayer; MUHEG, (11-mercaptoundecyl)hexa(ethylene glycol); NHS, *N*-hydroxysuccinimide; PC3, androgen-independent human prostatic small cell carcinoma; LnCaP, androgen-sensitive human prostate adenocarcinoma cells; RPMI, Roswell Park Memorial Institute; CCD, charged coupled device; PLSR, partial least squares regression; RMSE, root mean square error; LSPR, localized surface plasmon resonance; LOD, limit of detection

■ REFERENCES

(1) Apweiler, R.; Hermjakob, H.; Sharon, N. On the Frequency of Protein Glycosylation, as Deduced from Analysis of the SWISS-PROT Database. *Biochim. Biophys. Acta* **1999**, *1473*, 4−8.

(2) Lebrilla, C. B.; An, H. J. The Prospects of Glycan Biomarkers for the Diagnosis of Diseases. *Mol. BioSyst.* **2009**, *5*, 17−20.

(3) Fuster, M. M.; Esko, J. D. The Sweet and Sour of Cancer: Glycans as Novel Therapeutic Targets. *Nat. Rev. Cancer* **2005**, *5*, 526−542.

(4) Pinho, S. S.; Reis, C. A. Glycosylation in Cancer: Mechanisms and Clinical Implications. *Nat. Rev. Cancer* **2015**, *15*, 540−555.

(5) Scott, E.; Elliott, D. J.; Munkley, J. Tumour Associated Glycans: A Route to Boost Immunotherapy? *Clin. Chim. Acta* **2020**, *502*, 167−173.

(6) Zhou, L.; Wang, Y.; Xing, R.; Chen, J.; Liu, J.; Li, W.; Liu, Z. Orthogonal Dual Molecularly Imprinted Polymer-Based Plasmonic

Immunosandwich Assay: A Double Characteristic Recognition Strategy for Specific Detection of Glycoproteins. *Biosens. Bioelectron.* **2019**, *145*, 111729.
(7) Baker, M. Antibody Anarchy: A Call to Order. *Nature* **2015**, *527*, 545−551.
(8) Baker, M. Reproducibility Crisis: Blame It on the Antibodies. *Nature* **2015**, *521*, 274−276.
(9) Bertok, T.; Klukova, L.; Sediva, A.; Kasák, P.; Semak, V.; Micusik, M.; Omastova, M.; Chovanová, L.; Vlček, M.; Imrich, R.; Vikartovska, A.; Tkac, J. Ultrasensitive Impedimetric Lectin Biosensors with Efficient Antifouling Properties Applied in Glycoprofiling of Human Serum Samples. *Anal. Chem.* **2013**, *85*, 7324−7332.
(10) Furukawa, J.-i.; Fujitani, N.; Shinohara, Y. Recent Advances in Cellular Glycomic Analyses. *Biomolecules* **2013**, *3*, 198−225.
(11) Gabius, H. J.; André, S.; Jiménez-Barbero, J.; Romero, A.; Solís, D. From Lectin Structure to Functional Glycomics: Principles of the Sugar Code. *Trends Biochem. Sci.* **2011**, *36*, 298−313.
(12) Oliveira, C.; Teixeira, J. A.; Domingues, L. Recombinant Lectins: An Array of Tailor-Made Glycan-Interaction Biosynthetic Tools. *Crit. Rev. Biotechnol.* **2013**, *33*, 66−80.
(13) Deng, Y.; Yue, X.; Hu, H.; Zhou, X. A New Analytical Experimental Setup Combining Quartz Crystal Microbalance with Surface Enhancement Raman Spectroscopy and Its Application in Determination of Thrombin. *Microchem. J.* **2017**, *132*, 385−390.
(14) Fatisson, M.; Domingos, R. F.; Wilkinson, K. J.; Tufenkji, N. Deposition of TiO2 Nanoparticles onto Silica Measured Using a Quartz Crystal Microbalance with Dissipation Monitoring. *Langmuir* **2009**, *25*, 6062−6069.
(15) Chen, Z. M.; Wang, Y.; Du, X. Y.; Sun, J. J.; Yang, S. Temperature-Alternated Electrochemical Aptamer-Based Biosensor for Calibration-Free and Sensitive Molecular Measurements in an Unprocessed Actual Sample. *Anal. Chem.* **2021**, *93*, 7843−7850.
(16) Famulok, M.; Mayer, G. Aptamer Modules as Sensors and Detectors. *Acc. Chem. Res.* **2011**, *44*, 1349−1358.
(17) Langer, J.; de Aberasturi, D. J.; Aizpurua, J.; Alvarez-Puebla, R. A.; Auguié, B.; Baumberg, J. J.; Bazan, G. C.; Bell, S. E. J.; Boisen, A.; Brolo, A. G.; et al. Present and Future of Surface-Enhanced Raman Scattering. *ACS Nano* **2020**, *14*, 28−117.
(18) Siegel, R. L.; Miller, K. D.; Fuchs, H. E.; Jemal, A. Cancer Statistics, 2022. *Ca-Cancer J. Clin.* **2022**, *72*, 7−33.
(19) Tabarés, G.; Radcliffe, C. M.; Barrabés, S.; Ramírez, M.; Aleixandre, N.; Hoesel, W.; Dwek, R. A.; Rudd, P. M.; Peracaula, R.; de Llorens, R. Different Glycan Structures in Prostate-Specific Antigen from Prostate Cancer Sera in Relation to Seminal Plasma PSA. *Glycobiology* **2006**, *16*, 132−145.
(20) Matsumoto, K.; Yokote, H.; Arao, T.; Maegawa, M.; Tanaka, K.; Fujita, Y.; Shimizu, C.; Hanafusa, T.; Fujiwara, Y.; Nishio, K. N-Glycan Fucosylation of Epidermal Growth Factor Receptor Modulates Receptor Activity and Sensitivity to Epidermal Growth Factor Receptor Tyrosine Kinase Inhibitor. *Cancer Sci.* **2008**, *99*, 1611−1617.
(21) Saldova, R.; Fan, Y.; Fitzpatrick, J. M.; Watson, R. W. G.; Rudd, P. M. Core Fucosylation and A2−3 Sialylation in Serum N-Glycome Is Significantly Increased in Prostate Cancer Comparing to Benign Prostate Hyperplasia. *Glycobiology* **2011**, *21*, 195−205.
(22) Gilgunn, S.; Conroy, P. J.; Saldova, R.; Rudd, P. M.; O'Kennedy, R. J. Aberrant PSA Glycosylation - A Sweet Predictor of Prostate Cancer. *Nat. Rev. Urol.* **2013**, *10*, 99−107.
(23) Hsiao, J. J.; Smits, M. M.; Ng, B. H.; Lee, J.; Wright, M. E. Discovery Proteomics Defines Androgen-Regulated Glycoprotein Networks in Prostate Cancer Cells, as Well as Putative Biomarkers of Prostatic Diseases. *Sci. Rep.* **2021**, *11*, 22208.
(24) Aurilio, G.; Cimadamore, A.; Mazzucchelli, R.; Lopez-Beltran, A.; Verri, E.; Scarpelli, M.; Massari, F.; Cheng, L.; Santoni, M.; Montironi, R. Androgen Receptor Signaling Pathway in Prostate Cancer: From Genetics to Clinical Applications. *Cells* **2020**, *9*, 2653.
(25) Indrasekara, A. S. D. S.; Meyers, S.; Shubeita, S.; Feldman, L. C.; Gustafsson, T.; Fabris, L. Gold Nanostar Substrates for SERS-Based Chemical Sensing in the Femtomolar Regime. *Nanoscale* **2014**, *6*, 8891−8899.
(26) Villa, J. E. L.; Garcia, I.; Jimenez de Aberasturi, D.; Pavlov, V.; Sotomayor, M. D. P. T.; Liz-Marzán, L. M. SERS-Based Immunoassay for Monitoring Cortisol-Related Disorders. *Biosens. Bioelectron.* **2020**, *165*, 112418.
(27) Formisano, N.; Jolly, P.; Bhalla, N.; Cromhout, M.; Flanagan, S. P.; Fogel, R.; Limson, J. L.; Estrela, P. Optimisation of an Electrochemical Impedance Spectroscopy Aptasensor by Exploiting Quartz Crystal Microbalance with Dissipation Signals. *Sens. Actuators, B* **2015**, *220*, 369−375.
(28) Lenzi, E.; Jimenez De Aberasturi, D.; Liz-Marzán, L. M. Surface-Enhanced Raman Scattering Tags for Three-Dimensional Bioimaging and Biomarker Detection. *ACS Sens.* **2019**, *4*, 1126−1137.
(29) Serna, S.; Artschwager, R.; Pérez-Martínez, D.; Lopez, R.; Reichardt, N. C. A Versatile Urea Type Linker for Functionalizing Natural Glycans and Its Validation in Glycan Arrays. *Chem. -Eur. J.* **2023**, *29*, No. e202301494.
(30) Shibuya, N.; Goldstein, I. J.; Broekaert, W. F.; Nsimba-Lubaki, M.; Peeters, B.; Peumans, W. J. The Elderberry (Sambucus Nigra L.) Bark Lectin Recognizes the Neu5Ac(Alpha 2−6)Gal/GalNAc Sequence. *J. Biol. Chem.* **1987**, *262*, 1596−1601.
(31) Fujihashi, M.; Peapus, D. H.; Kamiya, N.; Nagata, Y.; Miki, K. Crystal Structure of Fucose-Specific Lectin from Aleuria Aurantia Binding Ligands at Three of Its Five Sugar Recognition Sites. *Biochemistry* **2003**, *42*, 11093−11099.
(32) Xiao, M.; Xie, K.; Dong, X.; Wang, L.; Huang, C.; Xu, F.; Xiao, W.; Jin, M.; Huang, B.; Tang, Y. Ultrasensitive Detection of Avian Influenza A (H7N9) Virus Using Surface-Enhanced Raman Scattering-Based Lateral Flow Immunoassay Strips. *Anal. Chim. Acta* **2019**, *1053*, 139−147.
(33) Zhang, L.; Salmain, M.; Liedberg, B.; Boujday, S. Naked Eye Immunosensing of Food Biotoxins Using Gold Nanoparticle-Antibody Bioconjugates. *ACS Appl. Nano Mater.* **2019**, *2*, 4150−4158.
(34) García-Álvarez, R.; Hadjidemetriou, M.; Sánchez-Iglesias, A.; Liz-Marzán, L. M.; Kostarelos, K. In Vivo Formation of Protein Corona on Gold Nanoparticles. the Effect of Their Size and Shape. *Nanoscale* **2018**, *10*, 1256−1264.
(35) Fogel, R.; Mashazi, P.; Nyokong, T.; Limson, J. Critical Assessment of the Quartz Crystal Microbalance with Dissipation as an Analytical Tool for Biosensor Development and Fundamental Studies: Metallophthalocyanine−Glucose Oxidase Biocomposite Sensors. *Biosens. Bioelectron.* **2007**, *23*, 95−101.
(36) Chen, Q.; Tang, W.; Wang, D.; Wu, X.; Li, N.; Liu, F. Amplified QCM-D Biosensor for Protein Based on Aptamer-Functionalized Gold Nanoparticles. *Biosens. Bioelectron.* **2010**, *26*, 575−579.
(37) Zheng, B.; Cheng, S.; Liu, W.; Lam, M. H. W.; Liang, H. Small Organic Molecules Detection Based on Aptamer-Modified Gold Nanoparticles-Enhanced Quartz Crystal Microbalance with Dissipation Biosensor. *Anal. Biochem.* **2013**, *438*, 144−149.
(38) Zhang, W. M.; Leinonen, J.; Kalkkinen, N.; Dowell, B.; Stenman, U. H. Purification and Characterization of Different Molecular Forms of Prostate-Specific Antiqen in Human Seminal Fluid. *Clin. Chem.* **1995**, *41*, 1567−1573.
(39) Chen, Z.; Lei, Y.; Chen, X.; Wang, Z.; Liu, J. An Aptamer Based Resonance Light Scattering Assay of Prostate Specific Antigen. *Biosens. Bioelectron.* **2012**, *36*, 35−40.
(40) Jolly, P.; Formisano, N.; Tkáč, J.; Kasák, P.; Frost, C. G.; Estrela, P. Label-Free Impedimetric Aptasensor with Antifouling Surface Chemistry: A Prostate Specific Antigen Case Study. *Sens. Actuators, B* **2015**, *209*, 306−312.
(41) Rodriguez, M. C.; Kawde, A. N.; Wang, J. Aptamer Biosensor for Label-Free Impedance Spectroscopy Detection of Proteins Based on Recognition-Induced Switching of the Surface Charge. *Chem. Commun.* **2005**, 4267−4269.
(42) Osypova, A.; Thakar, D.; Dejeu, J.; Bonnet, H.; Van Der Heyden, A.; Dubacheva, G. V.; Richter, R. P.; Defrancq, E.; Spinelli, N.; Coche-Guérente, L.; Labbé, P. Sensor Based on Aptamer Folding

https://doi.org/10.1021/acssensors.4c01252
ACS Sens. 2024, 9, 4811−4821

to Detect Low-Molecular Weight Analytes. *Anal. Chem.* **2015**, *87*, 7566−7574.
(43) Easley, A. D.; Ma, T.; Eneh, C. I.; Yun, J.; Thakur, R. M.; Lutkenhaus, J. L. A Practical Guide to Quartz Crystal Microbalance with Dissipation Monitoring of Thin Polymer Films. *J. Polym. Sci.* **2022**, *60*, 1090−1107.
(44) Matatagui, D.; Fontecha, J.; Fernández, M. J.; Oliver, M. J.; Hernando-García, J.; Sánchez-Rojas, J. L.; Gràcia, I.; Cané, C.; Santos, J. P.; Horrillo, M. C. Comparison of Two Types of Acoustic Biosensors to Detect Immunoreactions: Love-Wave Sensor Working in Dynamic Mode and QCM Working in Static Mode. *Sens. Actuators, B* **2013**, *189*, 123−129.
(45) Ma, W.; Liu, L.; Xu, Y.; Wang, L.; Chen, L.; Yan, S.; Shui, L.; Wang, Z.; Li, S. A Highly Efficient Preconcentration Route for Rapid and Sensitive Detection of Endotoxin Based on an Electrochemical Biosensor. *Analyst* **2020**, *145*, 4204−4211.
(46) Choi, J. H.; Kim, H. S.; Choi, J. W.; Hong, J. W.; Kim, Y. K.; Oh, B. K. A Novel Au-Nanoparticle Biosensor for the Rapid and Simple Detection of PSA Using a Sequence-Specific Peptide Cleavage Reaction. *Biosens. Bioelectron.* **2013**, *49*, 415−419.
(47) Pan, L. H.; Kuo, S. H.; Lin, T. Y.; Lin, C. W.; Fang, P. Y.; Yang, H. W. An Electrochemical Biosensor to Simultaneously Detect VEGF and PSA for Early Prostate Cancer Diagnosis Based on Graphene Oxide/SsDNA/PLLA Nanoparticles. *Biosens. Bioelectron.* **2017**, *89*, 598−605.
(48) Haga, Y.; Uemura, M.; Baba, S.; Inamura, K.; Takeuchi, K.; Nonomura, N.; Ueda, K. Identification of Multisialylated LacdiNAc Structures as Highly Prostate Cancer Specific Glycan Signatures on PSA. *Anal. Chem.* **2019**, *91*, 2247−2254.
(49) Rebello, R. J.; Oing, C.; Knudsen, K. E.; Loeb, S.; Johnson, D. C.; Reiter, R. E.; Gillessen, S.; Van der Kwast, T.; Bristow, R. G. Prostate Cancer. *Nat. Rev. Dis. Primers* **2021**, *7*, 9.
(50) Devlies, W.; Handle, F.; Devos, G.; Joniau, S.; Claessens, F. Preclinical Models in Prostate Cancer: Resistance to Ar Targeting Therapies in Prostate Cancer. *Cancers* **2021**, *13*, 915.
(51) Ideo, H.; Kondo, J.; Nomura, T.; Nonomura, N.; Inoue, M.; Amano, J. Study of Glycosylation of Prostate-Specific Antigen Secreted by Cancer Tissue-Originated Spheroids Reveals New Candidates for Prostate Cancer Detection. *Sci. Rep.* **2020**, *10*, 2708.
(52) Li, Y.; Tian, Y.; Rezai, T.; Prakash, A.; Lopez, M. F.; Chan, D. W.; Zhang, H. Simultaneous Analysis of Glycosylated and Sialylated Prostate-Specific Antigen Revealing Differential Distribution of Glycosylated Prostate-Specific Antigen Isoforms in Prostate Cancer Tissues. *Anal. Chem.* **2011**, *83*, 240−245.

https://doi.org/10.1021/acssensors.4c01252
ACS Sens. 2024, 9, 4811−4821